# Lattice Boltzmann model for a steady radiative transfer equation

Hong-Liang Yi,* Feng-Ju Yao, and He-Ping Tan†
*School of Energy Science and Engineering, Harbin Institute of Technology, Harbin 150001, People's Republic of China*
(Received 25 April 2016; revised manuscript received 4 July 2016; published 18 August 2016)

A complete lattice Boltzmann model (LBM) is proposed for the steady radiative transfer equation (RTE). The RTE can be regarded as a pure convection equation with a source term. To derive the expressions for the equilibrium distribution function and the relaxation time, an artificial isotropic diffusion term is introduced to form a convection-diffusion equation. When the dimensionless relaxation time has a value of 0.5, the lattice Boltzmann equation (LBE) is exactly applicable to the original steady RTE. We also perform a multiscale analysis based on the Chapman-Enskog expansion to recover the macroscopic RTE from the mesoscopic LBE. The D2Q9 model is used to solve the LBE, and the numerical results obtained by the LBM are comparable to the results obtained by other methods or analytical solutions, which demonstrates that the proposed model is highly accurate and stable in simulating multidimensional radiative transfer. In addition, we find that the convergence rate of the LBM depends on the transport properties of RTE: for diffusion-dominated RTE with a large optical thickness, the LBM shows a second-order convergence rate in space, while for convection-dominated RTE with a small optical thickness, a lower convergence rate is observed.

DOI: 10.1103/PhysRevE.94.023312

## I. INTRODUCTION

The radiative transfer equation (RTE) describes how photons propagate through random or participating media that scatter and absorb photons as well as emit photons. The radiative transfer equation has broad applications in thermal fields associated with high-temperature environments, such as astrophysics, atmospheric science, biomedical optics, and nuclear reactor physics, among others. Numerical simulation is an important tool for investigating the radiative transfer problem, and many numerical methods have been developed, such as the Monte Carlo method (MCM) [1–3], the zonal method [4,5], the spherical harmonics method ($P_N$) [6], the discrete-ordinates method (DOM) [7–11], the finite-volume method (FVM) [12,13], the finite-element method (FEM) [14,15], and the meshless method [16,17]. The MCM and zonal method are based on tracing the ray trajectory of radiation and can be regarded as benchmark methods with high computational accuracy. However, they are often time consuming even for relatively simple problems. The DOM, FVM, FEM, and meshless methods are based on global discretizations of the RTE and have the advantages of ease, efficiency, and flexibility to deal with multidimensional complex radiative transfer problems. However, these schemes suffer greatly from the instability caused by the convection-dominated property of the RTE with a small optical thickness.

Differing greatly from the numerical methods mentioned above, the lattice Boltzmann method (LBM) is a kinetic-based numerical model that has attracted a good amount of attention in the recent two decades or more. It has played an active role in solving a vast range of transport problems, including magnetohydrodynamic flow [18–20], multiphase flows [21–24], electrokinetic flows [25,26], electro-osmotic flows [27–29], electroconvection [30], heat transfer in a nanofluid [31–34], and the phase change problem [35–38]. Compared to the traditional computational fluid dynamics method based on the macroscopic continuum equations, owing to its mesoscopic nature, LBM offers some distinct advantages. It allows for a simple calculation procedure, high parallelism, and easy implementation of complex boundary conditions including a moving boundary, and it is highly adaptable to coupled multiphysics problems.

In recent years, some useful attempts have been made to solve radiative transfer problems using LBM. Mishra *et al.* [39,40] developed a lattice Boltzmann formulation for the analysis of radiative heat transfer problems in a participating medium. However, the method had some assumptions: scattering was assumed to be isotropic; the polar direction was isotropic and the angular dependence of intensity was only in the azimuthal direction; the particle distribution functions streamed only in finite discrete directions; and the fictitious speed of light was equal to the information propagating velocity, which caused a large total error. Ma *et al.* [41] derived macroscopic conservation equations of radiation energy and radiation momentum based on radiation hydrodynamics, and developed a lattice Boltzmann equation (LBE) framework to solve the one-dimensional radiative transfer problem. Bindra *et al.* [42] extended the method to two-dimensional radiative or neutron transport problems, in which particle distribution functions streamed only in a limited number of discrete directions. Zhang *et al.* [43] used a forward differencing scheme to rewrite the radiative transfer equation in the form of a lattice Boltzmann equation for solving one-dimensional transient radiative transfer. In all these works, the results were obtained with only a first-order convergence rate. Strictly speaking, LBM is not only a grid discretization scheme, but also a means of mathematical modeling. However, most of these existing works only use it as a grid discretization scheme, and do not build a rigorous mesoscopic lattice Boltzmann model for the radiative transfer equation. On the other hand, in the lattice Boltzmann model for physical problems, the determination of the collision operator is the key, and the relaxation time and equilibrium distribution function must be derived to determine the collision operator. However, there is no strict derivation of

*yihongliang@hit.edu.cn
†tanheping@hit.edu.cn

 

these properties. The evolution equation for LBM includes two separate steps, i.e., collision and streaming, and in all the above works the streaming direction is considered to be the direction of radiative transfer. This prevents the extension of LBM to multidimensional radiative transfer problems with high angular resolution. Unless the optical thickness assumption is satisfied, enough discrete directions must be ensured in most of numerical models to mitigate the ray effect and improve the calculation accuracy for a radiative transfer problem. Quite recently, Mink *et al.* [44] developed a three-dimensional LBM for radiative transfer based on the $P_1$ approximation of RTE and performed a Chapman-Enskog analysis of the proposed algorithm. However, the $P_1$ method approximates the RTE as a macroscopic diffusion equation, and the corresponding LBM is applicable only to radiative transfer in an optically thick media. Therefore, in the strictest sense, none of these works establish a complete LB model for the radiation transfer problem.

If the direction vector of radiative transfer is regarded as the velocity vector, the radiative transfer equation can be taken as a convection equation without the diffusion term that may result in a nonphysical oscillation of numerical solutions. Recently, researchers have proposed a variety of lattice Boltzmann models for the convection-diffusion equations (CDEs) [45–52]. So far no work on the lattice Boltzmann modeling of such a convection equation as the radiative transfer equation has been reported. However, inspiration from previous work on the LBM for the convection-diffusion equation may offer the possibility of establishing the complete lattice Boltzmann model for the radiative transfer equation.

In this work, we establish a lattice Boltzmann model (LBM) for a two-dimensional steady RTE based on the Chapman-Enskog expansion and present an efficient algorithm for the implementation of the model. In Sec. II, we provide the steady RTE first, and then propose the corresponding LBM, including the derivation of an LBE for the radiation intensity field at each direction of radiative transfer, a Chapman-Enskog analysis of the LBE, and the implementation of boundary conditions. Section III describes the numerical solution procedure in detail. In Sec. IV, we examine three two-dimensional test cases of radiative transfer problems in participating media to verify the numerical accuracy, and evaluate the convergence property of the LBM in detail. In addition, in this section we investigate the radiative transfer in a square enclosure with a Gaussian shaped emissive field and a coupled conduction and radiation problem. Conclusions are drawn in the last section.

## II. MATHEMATIC FORMULATIONS

In this part, we first provide the governing equation for radiative transfer. Then, we establish the corresponding lattice Boltzmann equation for the radiation intensity field. Next, we perform a Chapman-Enskog analysis of the LBE. Finally, we present an implementation of boundary conditions.

### A. Radiative transfer equation

The radiation intensity field is obtained by solving the radiative transfer equation (RTE). The steady RTE for an absorbing, emitting, and scattering gray medium can be written as

$$\frac{\partial I(\mathbf{r},\mathbf{s})}{\partial s} = \mathbf{s}\cdot\nabla I(\mathbf{r},\mathbf{s}) = -\beta I(\mathbf{r},\mathbf{s}) + S(\mathbf{r},\mathbf{s}), \tag{1}$$

where $I$ is the radiation intensity, $\mathbf{r}$ is the location vector, and $\mathbf{s}$ is the unit direction vector of radiation transfer. $\beta$ is the extinction coefficient, defined as $\beta = \kappa_a + \kappa_s$, where $\kappa_a$ is the absorption coefficient, and $\kappa_s$ is the scattering coefficient. $S$ is the source function accounting for the thermal emission of media and in-scattering radiation, given by

$$S = \kappa_a n^2 I_b(\mathbf{r}) + \frac{\kappa_s}{4\pi}\int_{4\pi} I(\mathbf{r},\mathbf{s}')\Phi(\mathbf{s}',\mathbf{s})d\Omega', \tag{2}$$

where $I_b$ is the blackbody radiation intensity, expressed as $I_b = \sigma T^4/\pi$, $n$ is the refractive index of the medium, $\Phi$ is the scattering phase function, and $\Omega$ is the solid angle.

Equation (1) is subject to the boundary condition

$$I(\mathbf{r}_w,\mathbf{s}) = \varepsilon_w n^2 I_b(\mathbf{r}_w) + \frac{1-\varepsilon_w}{\pi}\int_{\mathbf{n}_w\cdot\mathbf{s}'<0} I(\mathbf{r}_w,\mathbf{s}')|\mathbf{n}_w\cdot\mathbf{s}'|d\Omega', \tag{3}$$

where we have limited ourselves to an enclosure with opaque, diffusely emitting and diffusely reflecting walls. The extension of Eq. (3) to more complicated boundary conditions is straightforward. $\varepsilon_w$ is the wall emissivity, and $\mathbf{n}_w$ is the unit normal vector of the wall.

Equation (1) is solved for a set of $M$ different directions, $\mathbf{s}_i, i = 1,2,\ldots,M$, and the direction integrals in Eq. (2) and Eq. (3) are replaced by numerical quadrature. Thus Eq. (1) is approximated by a set of $M$ equations,

$$\mathbf{s}_i\cdot\nabla I(\mathbf{r},\mathbf{s}_i) = -\beta I(\mathbf{r},\mathbf{s}_i) + S(\mathbf{r},\mathbf{s}_i), \quad i = 1,2,\ldots,M, \tag{4}$$

subject to the boundary conditions

$$I(\mathbf{r}_w,\mathbf{s}_i) = \varepsilon_w n^2 I_b(\mathbf{r}_w) + \frac{1-\varepsilon_w}{\pi}\sum_{\boldsymbol{n}_w\cdot\boldsymbol{s}_j<0} I(\mathbf{r},\mathbf{s}_j)|\mathbf{n}_w\cdot\mathbf{s}_j|w_j, \quad \mathbf{n}_w\cdot\mathbf{s}_i > 0, \tag{5}$$

where

$$S(\mathbf{r},\mathbf{s}_i) = \kappa_a n^2 I_b(\mathbf{r}) + \frac{\kappa_s}{4\pi}\sum_{j=1}^{M} I(\mathbf{r},\mathbf{s}_j)\Phi(\mathbf{s}_j,\mathbf{s}_i)w_j, \tag{6}$$

and $w_j$ is the quadrature weight associated with the direction $\mathbf{s}_j$.

We obtain the radiative intensity field by solving Eq. (4). In the investigation of a radiative transfer problem, the incident radiation $G$ and the radiative heat flux $q_R$ are two important physical quantities. Once the distribution of radiation intensity is obtained, the distribution of the incident radiation $G$ can be calculated by

$$G(\boldsymbol{r}) = \int_{4\pi} I(\mathbf{r},\mathbf{s})d\Omega, \tag{7}$$

and the radiative heat flux in the $x$ and $y$ directions can be calculated from

$$q_{R,x}(\mathbf{r}) = \int_{4\pi} I(\mathbf{r},\mathbf{s})\cdot(\mathbf{s}\cdot\boldsymbol{e}_x)d\Omega, \tag{8}$$

$$q_{R,y}(\mathbf{r}) = \int_{4\pi} I(\mathbf{r},\mathbf{s})\cdot(\mathbf{s}\cdot\boldsymbol{e}_y)d\Omega. \tag{9}$$

### B. Lattice Boltzmann model

#### 1. Lattice Boltzmann equation

As shown in Eq. (1), if the direction vector of radiation transfer $\mathbf{s}$ can be taken as a velocity vector, the radiative transfer equation is a convection equation without the diffusion term. From the derivation of LBEs for convection-diffusion equations [45–52], the relaxation time of the LBM is related to the diffusion coefficient of the CDE. Thus, to obtain an expression of the relaxation time, we add a positive artificial diffusion term to the right side of Eq. (1), leading to

$$\mathbf{s}\cdot\nabla I(\mathbf{r},\mathbf{s}) = -\beta I(\mathbf{r},\mathbf{s}) + S(\mathbf{r},\mathbf{s}) + \alpha\nabla[\nabla I(\mathbf{r},\mathbf{s})], \quad (10)$$

where $\alpha$ is the diffusion coefficient. Once $\alpha$ is set to zero, Eq. (10) is reduced to a radiative transfer equation. For the direction $\mathbf{s}_k (k = 1,2,\ldots,M)$ of radiative transfer, Eq. (10) is written as

$$\mathbf{s}_k\cdot\nabla I(\mathbf{r},\mathbf{s}_k) = -\beta I(\mathbf{r},\mathbf{s}_k) + S(\mathbf{r},\mathbf{s}_k) + \alpha\nabla[\nabla I(\mathbf{r},\mathbf{s}_k)], \quad (11)$$

where

$$\mathbf{s}_k = \boldsymbol{i}\mu_k + \boldsymbol{j}\eta_k + \boldsymbol{k}\xi_k, \quad (12)$$

in which $\mu_k,\eta_k$, and $\xi_k$ are the direction cosines of $\mathbf{s}_k$.

We begin deriving the corresponding lattice Boltzmann equation from Eq. (11). The two-dimensional problem is considered, so let

$$\mathbf{U} = [\mu_k,\eta_k]^T, \quad (13)$$

$$\mathbf{I} = \begin{pmatrix}1,0\\0,1\end{pmatrix}, \quad (14)$$

$$F(\mathbf{r},\mathbf{s}_k) = S(\mathbf{r},\mathbf{s}_k) - \beta I(\mathbf{r},\mathbf{s}_k). \quad (15)$$

Then we rewrite Eq. (11) as

$$\nabla\cdot(I\mathbf{U}) = \alpha\nabla\cdot[\nabla\cdot(I\mathbf{I})] + F. \quad (16)$$

The corresponding evolution equation of the LB model is

$$f_i(\mathbf{r}+\mathbf{e}_i\Delta t, t+\Delta t) - f_i(\mathbf{r},t) = -\frac{1}{\tau_i}\left[f_i(\mathbf{r},t) - f_i^{\mathrm{eq}}(\mathbf{r},t)\right] + \Delta t F_i(\mathbf{r},t) + \frac{(\Delta t)^2}{2}\partial_t F_i(\mathbf{r},t), \quad (17)$$

where $\{\mathbf{e}_i = c\mathbf{I}, c = \Delta x/\Delta t, i = 0,\ldots,8\}$ is a set of discrete velocities for the D2Q9 lattice model shown in Fig. 1, $\Delta t$ is the time step, $\tau_i$ is the dimensionless relaxation time, and $f_i(\mathbf{r},t)$ and $f_i^{\mathrm{eq}}(\mathbf{r},t)$ represent the local particle distribution function and equilibrium distribution function at position $\mathbf{r}$ and time $t$.

The key point of using Eq. (17) to solve Eq. (16) is to construct proper expressions for $f_i^{\mathrm{eq}}(\mathbf{r},t)$ and $F_i(\mathbf{r},t)$. Based on the work [50], the equilibrium distribution function $f_i^{\mathrm{eq}}(\mathbf{r},t)$ and source term $F_i(\mathbf{r},t)$ are taken as

$$f_i^{\mathrm{eq}} = \begin{cases}(w_0-1)I & i=0\\ w_i\left(I + \frac{\mathbf{e}_i\cdot I\mathbf{U}}{c_s^2}\right) & i = 1\text{–}8\end{cases}, \quad (18)$$

$$F_i = \overline{w_i}F, \quad (19)$$

in which $w_i$ and $\overline{w_i}$ are the weights of the equilibrium distribution function and the source term distribution function for different directions, respectively. For the D2Q9 lattice model, $w_i$ and $\overline{w_i}$ have the following values:

$$w_i = \begin{cases}4/9 & i=0\\ 1/9 & i=1\text{–}4\\ 1/36 & i=5\text{–}8\end{cases}, \quad (20)$$

$$\overline{w_i} = \begin{cases}0 & i=0\\ 1/6 & i=1\text{–}4\\ 1/12 & i=5\text{–}8\end{cases}. \quad (21)$$

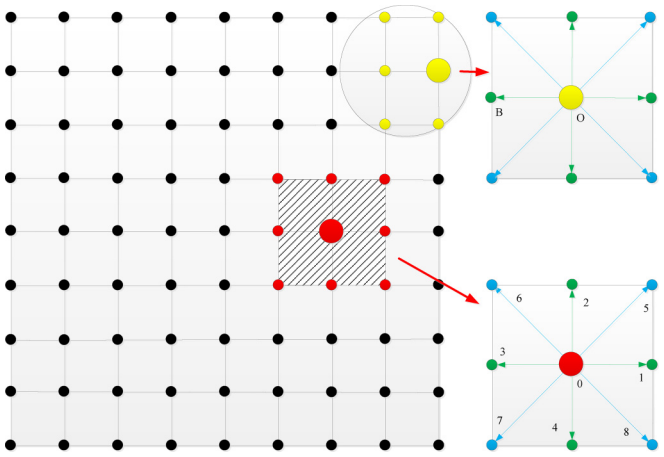


FIG. 1. D2Q9 lattice scheme used for a 2D geometry in a lattice Boltzmann model.

For Eq. (16), following the scheme adopted in Ref. [50], we introduce one parameter to adjust the accuracy and stability of the present model. Thus the equilibrium distribution function and the source term are modified by

$$f_i^{\mathrm{eq}} = \begin{cases}(w_0-1)I & i=0\\ w_i\left(I + \frac{\mathbf{e}_i\cdot\delta I\mathbf{U}}{c_s^2}\right) & i = 1\text{–}8\end{cases}, \quad (22)$$

$$F_i = \overline{w_i}\delta F, \quad (23)$$

where $\delta$ is the adjustable parameter. With a judicious choice of the value of $\delta$, the stability and accuracy of the model can be greatly improved.

According to the Chapman-Enskog analysis detailed below, the dimensionless relaxation time can be obtained by

$$c_s^2\left(\tau_i - \tfrac{1}{2}\right)\Delta t = \alpha\delta, \quad (24)$$

where $\tau_i = 0.5$ when $\alpha$ is set to 0.

From Eqs. (22)–(24), we see that only relaxation time is related with the diffusion coefficient, not the equilibrium distribution function and source term. Therefore, the lattice Boltzmann equation, i.e., Eq. (17), with a relaxation time of 0.5 is just suitable to model the standard steady radiative transfer equation. The relaxation time of a radiative transfer problem is the same as that of fluid flow with zero shear viscosity [53].

The macroscopic variable $I$ can be obtained using

$$I = \sum_{i=1}^{8} f_i/(1-w_0). \quad (25)$$

### 2. Chapman-Enskog analysis

We perform a Chapman-Enskog analysis to recover the macroscopic radiative transfer equation with an artificial diffusion term [Eq. (16)] from the lattice Boltzmann equation [Eq. (17)]. The details are presented below.

Expanding the distribution functions and the time and space derivatives, we get

$$f_i = f_i^{(0)} + \varepsilon f_i^{(1)} + \varepsilon^2 f_i^{(2)}, \tag{26}$$

$$\nabla = \varepsilon \nabla_1, \tag{27}$$

$$\partial_t = \varepsilon \partial_{t1} + \varepsilon^2 \partial_{t2}, \tag{28}$$

$$F_i = \varepsilon F_i^{(1)}, \tag{29}$$

where $\varepsilon$ is a small expansion parameter.

By applying the Taylor expansion to Eq. (17), we have

$$\begin{aligned} &\Delta t D_i f_i + \frac{1}{2}\Delta t^2 D_i^2 f_i \\ &= -\frac{1}{\tau_i}\left[f_i - f_i^{\mathrm{eq}}\right] + \Delta t F_i + \frac{1}{2}\Delta t^2 \partial_t F_i, \end{aligned} \tag{30}$$

where $D_i = \varepsilon D_{1i} + \varepsilon^2 \partial_{t2}$ with $D_{1i} = \partial_{t1} + \mathbf{e}_i \cdot \nabla_1$.

Substituting Eqs. (26)–(29) into Eq. (30) gives

$$\begin{aligned} &(\varepsilon D_{1i} + \varepsilon^2 \partial_{t2})\left(f_i^{(0)} + \varepsilon f_i^{(1)} + \varepsilon^2 f_i^{(2)}\right) \\ &\quad + \frac{\Delta t}{2}(\varepsilon D_{1i} + \varepsilon^2 \partial_{t2})^2\left(f_i^{(0)} + \varepsilon f_i^{(1)} + \varepsilon^2 f_i^{(2)}\right) \\ &= -\frac{1}{\tau_i \Delta t}\left[\left(f_i^{(0)} + \varepsilon f_i^{(1)} + \varepsilon^2 f_i^{(2)}\right) - f_i^{\mathrm{eq}}\right] \\ &\quad + \varepsilon F_i^{(1)} + \frac{\Delta t}{2}(\varepsilon D_{1i} + \varepsilon^2 \partial_{t2})\varepsilon F_i^{(1)}, \end{aligned} \tag{31}$$

and by scale analysis, we obtain the equations in $\varepsilon^0$, $\varepsilon^1$, and $\varepsilon^2$:

$$\varepsilon^0 : f_i^{(0)} = f_i^{\mathrm{eq}}, \tag{32}$$

$$\varepsilon^1 : D_{1i} f_i^{(0)} = -\frac{1}{\tau_i \Delta t} f_i^{(1)} + F_i^{(1)}, \tag{33}$$

$$\begin{aligned} \varepsilon^2 : &D_{1i} f_i^{(1)} + \partial_{t2} f_i^{(0)} + \frac{\Delta t}{2} D_{1i}^2 f_i^{(0)} \\ &= -\frac{1}{\tau_i \Delta t} f_i^{(2)} + \frac{\Delta t}{2}\partial_{t1} F_i^{(1)}. \end{aligned} \tag{34}$$

Substituting Eq. (33) into Eq. (34) leads to

$$\begin{aligned} &\left(1 - \frac{1}{2\tau_i}\right) D_{1i} f_i^{(1)} + \partial_{t2} f_i^{(0)} + \frac{\Delta t}{2} D_{1i} F_i^{(1)} \\ &= -\frac{1}{\tau_i \Delta t} f_i^{(2)} + \frac{\Delta t}{2}\partial_{t1} F_i^{(1)}. \end{aligned} \tag{35}$$

In Eq. (17), $f_i, f_i^{\mathrm{eq}}$ [Eq. (22)] and $F_i$ [Eq. (23)] satisfy the following conditions:

$$\sum_i f_i = \sum_i f_i^{\mathrm{eq}} = 0, \tag{36}$$

$$\sum_i \mathbf{e}_i f_i^{\mathrm{eq}} = \delta I \mathbf{U}, \tag{37}$$

$$\sum_i \mathbf{e}_i \mathbf{e}_i f_i^{\mathrm{eq}} = c_s^2 I \mathbf{I}, \tag{38}$$

$$\sum_i F_i = \delta F, \tag{39}$$

$$\sum_i \mathbf{e}_i F_i = 0. \tag{40}$$

Summing Eqs. (33) and (35) over $i$, respectively, and using Eqs. (36)–(40), we obtain

$$\nabla_1 \cdot (\delta I \mathbf{U}) = \delta F^{(1)}, \tag{41}$$

$$\nabla_1 \cdot \left[\left(1 - \frac{1}{2\tau_i}\right)\sum_i \mathbf{e}_i f_i^{(1)}\right] = 0. \tag{42}$$

Using Eq. (33),

$$\begin{aligned} \sum_i \mathbf{e}_i f_i^{(1)} &= -\tau_i \Delta t \sum_i \mathbf{e}_i \left(D_{1i} f_i^{(0)} - F_i^{(1)}\right) \\ &= -\tau_i \Delta t \nabla_1 \cdot \left(c_s^2 I \mathbf{I}\right). \end{aligned} \tag{43}$$

Substituting Eq. (43) into Eq. (42) leads to

$$0 = \nabla_1 \cdot \left[c_s^2\left(\tau_i - \tfrac{1}{2}\right)\Delta t \nabla_1 \cdot (\mathbf{I} I)\right]. \tag{44}$$

Combining Eqs. (41) and (44) and taking

$$c s^2\left(\tau_i - \tfrac{1}{2}\right)\Delta t = \alpha \delta, \tag{45}$$

we can obtain

$$\delta \nabla \cdot (I \mathbf{U}) = \delta \alpha \nabla \cdot [\nabla \cdot (I \mathbf{I})] + \delta F. \tag{46}$$

Finally, Eq. (46) is divided by $\delta$, and the macroscopic radiative transfer equation with an artificial diffusion term [Eq. (16)] can be recovered. By setting the diffusion coefficient to zero, Eq. (16) is transformed into the standard steady RTE. With $\tau_i = 0.5$, the lattice Boltzmann equation, i.e., Eq. (17), combined with the boundary condition given below, can be used to model two-dimensional steady radiative transfer.

### 3. Boundary conditions

Corresponding to the radiative boundary condition [Eq. (5)] for steady RTE [Eq. (4)], the nonequilibrium extrapolation scheme discussed in Ref. [54] is applied for the LBE [Eq. (17)]. The distribution function on the boundary is composed of two parts, an equilibrium distribution function and a nonequilibrium distribution function,

$$f_\alpha(O,t) = f_\alpha^{\mathrm{eq}}(O,t) + f_\alpha^{\mathrm{neq}}(O,t), \tag{47}$$

where the equilibrium distribution function can be obtained by computing macroscopic physical quantities such as radiation intensity on the boundary from Eq. (22), and the nonequilibrium distribution function is replaced by the corresponding quantities on the neighboring position. Thus we have

$$f_\alpha(O,t) = f_\alpha^{\mathrm{eq}}(O,t) + \left[f_\alpha(B,t) - f_\alpha^{\mathrm{eq}}(B,t)\right], \tag{48}$$

where $O$ is the point at the boundary and $B$ is its adjacent point in the domain, as shown in Fig. 1.

## III. NUMERICAL SOLUTION PROCEDURE

The numerical solution procedure for calculating a macroscopic quantity, such as radiation intensity, is given as follows.

(1) Discretize the calculation domain using uniform grids. Set the input parameters, such as temperature distribution, extinction coefficient, wall emissivity, scattering albedo, and phase function, for the simulations.

(2) Initialize the radiation intensity field and set the dimensionless relaxation time of Eq. (17) to 0.5 for simulating a radiative transfer problem.

(3) Discretize the angular space into $M = N(N+2)$ transfer directions using the $S_N$ quadrature scheme [55] and calculate the corresponding direction cosines and quadrature weights for the different radiation transfer directions.

(4) Loop each angular direction for $m = 1, \ldots, M$.

(a) Calculate the equilibrium distribution function using Eq. (22) and the source term using Eq. (23).

(b) Solve the LBE for a radiative transfer equation using Eq. (17).

(c) Modify the particle distribution functions to satisfy the boundary conditions from Eq. (48).

(d) Obtain the radiative intensity at each discrete node.

(5) Obtain the radiative heat flux and incident radiation.

(6) Repeat steps (4) and (5) until the convergence criterion is satisfied.

Convergence is declared if the following criterion is satisfied:

$$\max\left(\left|\frac{G^{n+1}-G^{n}}{G^{n+1}}\right|\right) < 10^{-6}. \tag{49}$$

## IV. RESULTS AND DISCUSSIONS

To evaluate the numerical performance of the present LBM, we compare the results produced by the LBM with numerical solutions generated by other methods and investigate the convergence property of the LBM in space. We examine three test cases for two-dimensional (2D) radiative transfer problems for comparison. Next, we investigate a test case to illustrate the method's stability for radiative transfer, and finally we present an application of the proposed LBM to coupled radiation and conduction. Square media with side length $L = 1$ and refractive index $n = 1$ are considered. The quadrature scheme $S_6$ is used to discretize the angular space for all the cases.

### A. Purely absorbing medium in a black enclosure

The LBM is applied to simulate radiative transfer in a black square enclosure with a purely absorbing-emitting medium. We consider the extinction coefficients $\beta = 0.1$, 1, and 10. The medium is kept hot with a dimensionless temperature of 1, and all boundary walls are kept cold. In Fig. 2, the dimensionless radiative heat fluxes $\psi_R = q_w/\sigma T_{\max}^4$ are plotted for comparison. Uniform meshes of $40 \times 40$, $60 \times 60$, and $200 \times 200$ are required for spatial discretization of the media with $\beta = 0.1$, 1, and 10, respectively. In participating media with a larger extinction coefficient, the radiation energy is more strongly attenuated, which results in a greater change in intensity within a certain distance. In other words, media with larger extinction coefficients have a greater

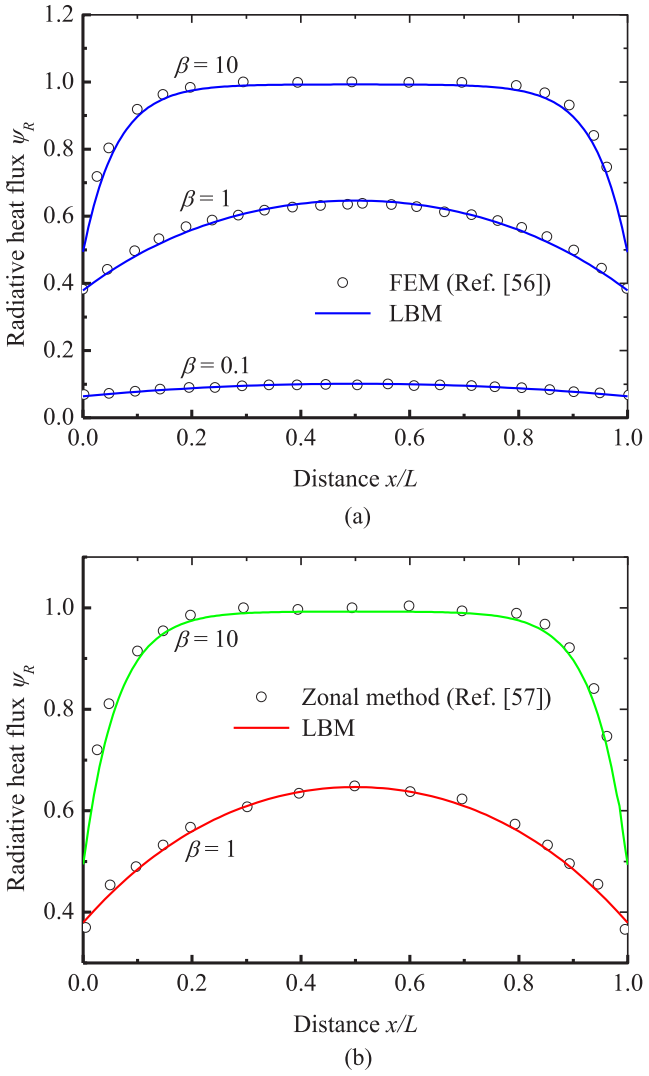


FIG. 2. Radiative heat flux along the $x$ direction in a purely absorbing medium with extinction coefficients $\beta = 0.1$, 1, and 10. (a) Comparison with the FEM, and (b) comparison with the zone method.

radiation intensity gradient due to more intense extinction of the radiation. Therefore, in order to achieve an accurate simulation, a relatively fine spatial discretization is needed for media with large extinction coefficients.

After a large number of numerical tests, we find that the adjustable parameter $\delta$ in Eqs. (22) and (23) is dependent on optical thickness ($\tau = \beta L$), time step ($\Delta t$), and lattice sound speed ($c_s$), and that $\delta = (a\tau + b)c_s^2\Delta t$ where $a = 0.75$ and $b = 1.65$. The adjustable parameter function is universal and can be applied to the radiative transfer problems in this work. In addition, it is also adequate for other classes of 2D radiative transfer problems, such as the radiative equilibrium problem and the coupled radiation and conduction problem discussed in Sec. IV F.

From the comparison in Fig. 2, we can see that the dimensionless radiative heat fluxes found by the LBM are in good agreement with the results obtained by an FEM [56] with $10 \times 10$ elements and a four-node $S_8$ approximation for $\beta = 0.1, 1\ \mathrm{m}^{-1}$ and an eight-node $S_8$ approximation for

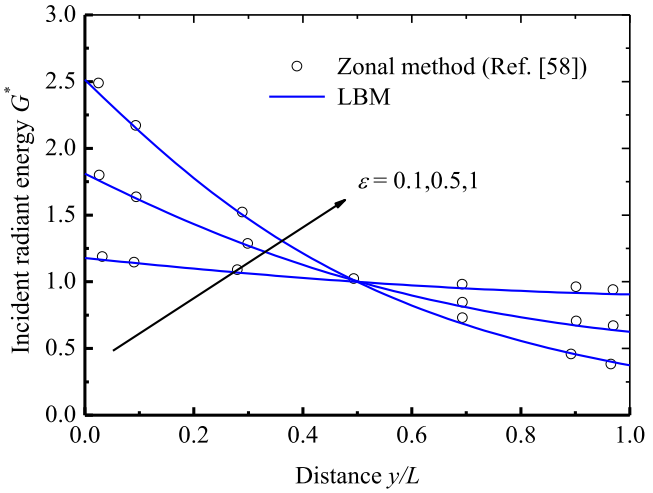


FIG. 3. The centerline incident radiation along the $y$ direction in an isotropically scattering medium with emissivities $\varepsilon = 0.1$, 0.5, and 1.

$\beta = 10\,\mathrm{m}^{-1}$ based on the even parity form of the RTE and zone method [57] with 225 volume elements and 60 surface segments, respectively. The maximum relative error is less than 2%.

### B. Purely scattering media in a gray enclosure

Radiative transfer in isotropically scattering media is simulated by LBM, and the incident radiation and radiative flux are predicted for wall emissivities of $\varepsilon_w = 0.1$, 0.5, and 1. In this case, a scattering albedo $\omega = 1$, and an extinction coefficient $\beta = 1$. The bottom wall of the considered medium is kept hot and its dimensionless temperature is set to 1, while the other three walls and the medium bounded by the square enclosure are kept cold.

Figure 3 plots the centerline dimensionless incident radiation $G^* = G/(\sigma T^4)$ and Fig. 4 plots the dimensionless radiative heat flux $\psi_R = q_w/\sigma T_{\max}^4$. The results obtained by the LBM and the zone method [58] with 225 volume elements and 60 surface segments are comparable, and the maximum relative errors are 1.85% and 1.05% for the centerline incident radiation and the radiative heat flux, respectively. It is worth noting that the maximum relative errors for incident radiation and radiative flux occur at the region adjacent to the wall and the corner of the medium with $\varepsilon_w = 1$, respectively. This is to be expected, since the larger the emissivity, the more intense the radiative energy absorbed at the walls, and the greater the gradient of radiation intensity at the regions adjacent to the walls or corners of the medium. Therefore, denser meshes are required to obtain more accurate results for the spatial discretization of the medium with greater emissivity. As shown in Fig. 4, for a $60 \times 60$ spatial grid, the maximum relative error of radiative flux at the region adjacent to the corner is 3.3%, while for the $120 \times 120$ spatial discretization, the maximum relative error is reduced to 1.05%.

### C. Anisotropically scattering medium in a black enclosure

The LBM is applied to solve radiative transfer in a black square enclosure with an absorbing, emitting, and anisotropically scattering medium. The extinction coefficient of the medium is $\beta = 1$. The F2 phase function is considered, given by Eq. (50) with an asymmetry factor of 0.669 72:

$$\mathbf{\Phi}(\mathbf{s},\mathbf{s}') = \sum_{j=0}^{8} C_j P_j(\mathbf{s}\cdot\mathbf{s}'). \tag{50}$$

Here, $P_j$ is the $j$th Legendre polynomial, and $C_j$ is the corresponding expansion coefficient: $C_0 = 1.0$, $C_1 = 2.009\,17$, $C_2 = 1.563\,39$, $C_3 = 0.674\,07$, $C_4 = 0.222\,15$, $C_5 = 0.047\,25$, $C_6 = 0.006\,71$, $C_7 = 0.000\,68$, and $C_8 = 0.000051\,7$.

Figure 5 illustrates the radiative flux $\psi_R = q_w/\sigma T_{\max}^4$ obtained by LBM and DOM [59] with $26 \times 26$ control volumes and an $S_{14}$ approximation along the bottom surface for three different values of the albedo $\omega$, specifically 0.0, 0.5, and 0.9. Figure 5 shows good agreement between the results from the two numerical methods, with a maximum relative error less than 2%.

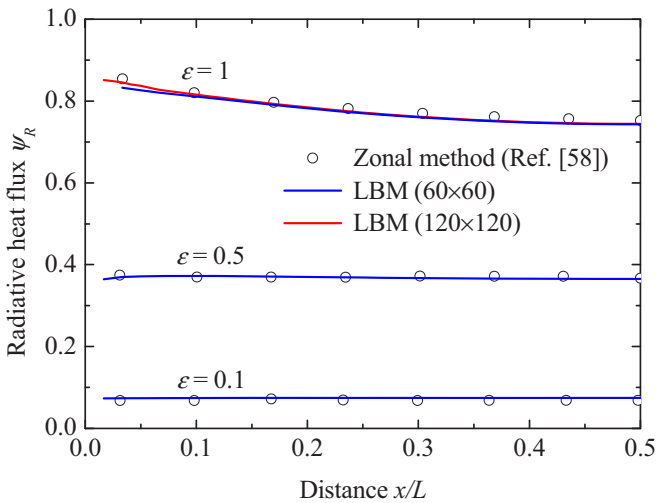


FIG. 4. Radiative heat flux along the $x$ direction in an isotropically scattering medium with emissivities $\varepsilon = 0.1$, 0.5, and 1.

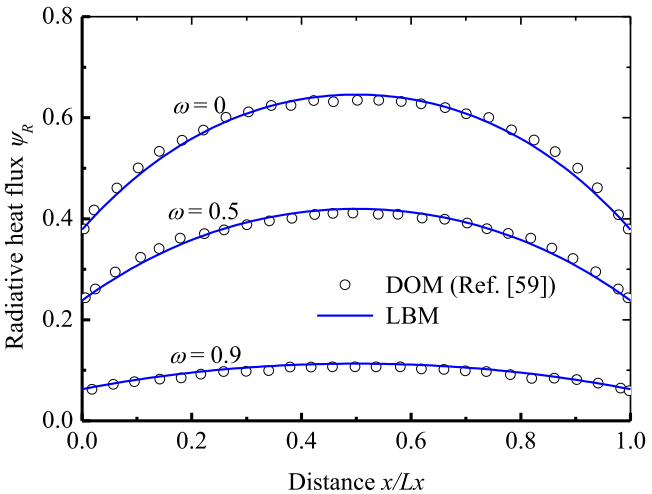


FIG. 5. Radiative heat flux along the $x$ direction in an anisotropically scattering medium with scattering albedos $\omega = 0$, 0.5, and 0.9.

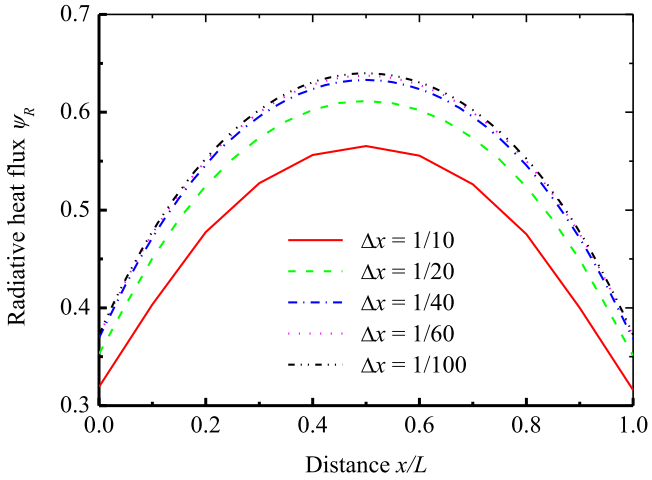


FIG. 6. Grid independence test for results from the LBM.

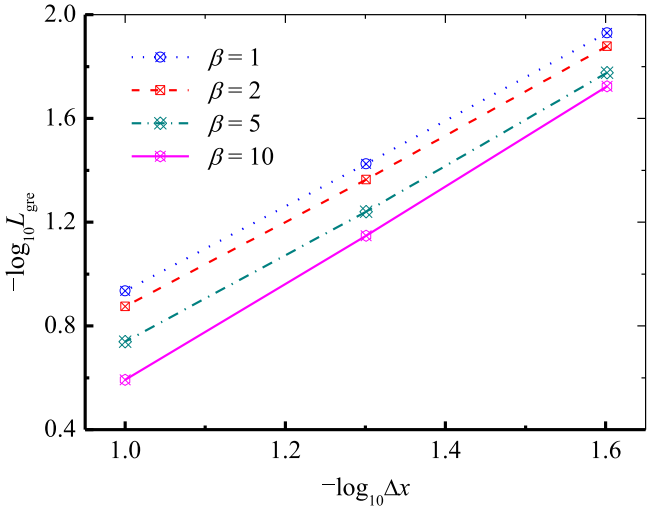


FIG. 7. Global relative errors of the lattice Boltzmann model with different lattice steps.

### D. Analysis of the convergence rate in space

From the above comparisons between the LBM and other numerical methods, we can see that the proposed LBM has good accuracy and excellent stability in the simulation of 2D steady radiative transfer under various working conditions. In this section, the spatial convergence property of the LBM is examined.

The order of convergence rate of the present LBM is evaluated using the equation [60]

$$\text{order} = \log_{10}(L^{h_1}/L^{h_2})/\log_{10}(h_1/h_2), \tag{51}$$

where $h_1$ and $h_2$ denote two different grid sizes and $L$ denotes numerical error. In our simulations, the global relative error $L_{\text{gre}}$ is used to test the accuracy of the present lattice Boltzmann model, which is defined as

$$L_{\text{gre}} = \frac{\sum_N |\varphi^n - \varphi^r|}{\sum_N |\varphi^r|}, \tag{52}$$

where $\varphi^n$ and $\varphi^r$ correspond to the numerical and reference solutions, respectively, for a basic scalar [here it is the dimensionless incident radiation $G^* = G/(\sigma T^4)$], and $N$ is the total number of lattice points in the whole domain. For this case, $\varphi^r$ takes the solutions under the refined lattices.

We first perform the grid independence test of results by the LBM, and the working condition is set to be $\varepsilon = 1$, $\omega = 0$, and $\beta = 1$. As shown in Fig. 6, when the grid is sparse, the results converge quickly with the grid. The finer the grid, the more slowly the results converge. The maximum relative error between $\Delta x = 1/40$ and $\Delta x = 1/60$ is 0.314%. The maximum relative error between $\Delta x = 1/60$ and $\Delta x = 1/100$ is 0.156%. We choose the grid numbers to be $Nx \times Ny = 8080, 120 \times 120, 200 \times 200$, and $320 \times 320$ for the reference solutions with $\beta = 1$, 2, 5, and 10, respectively.

To test the convergence rate of the present LBM, we carry out simulations at different lattice steps ($\Delta x = 1/10$ to 1/40). The global relative errors ($L_{\text{gre}}$) between the numerical results and the reference results are plotted in Fig. 7 with extinction coefficients $\beta = 1$, 2, 5, and $10\,\text{m}^{-1}$. The orders of the convergence rate estimated based on the relative errors $L_{\text{gre}}$ are 1.683, 1.713, 1.786, and 1.92 for $\beta = 1$, 2, 5, and $10\,\text{m}^{-1}$, respectively. The radiative transfer equation is a convection-dominated equation when the optical thickness ($\beta L$) is not large, for instance, $\beta L = 1$. The convection-dominated equation suffers from severe numerical instability, and the corresponding numerical solutions converge slowly with grid refinement. When the optical thickness is large, for instance, $\beta L = 10$, the radiation energy emitted from walls or media decays very rapidly over a short transfer distance, and the radiative transfer behavior shows significant diffusion characteristics. For the radiative transfer equation with strong diffusion characteristics, the numerical solutions converge rapidly with grid refinement. According to the above analysis, the spatial convergence rate of results increases with increasing optical thickness, as shown in Fig. 7, and it is expected that for the radiative transfer in media with an optical thickness greater than 10, the present LBM may have an approximate second-order convergence rate in space. In addition, we also notice that the global relative errors $L_{\text{gre}}$ for a larger extinction coefficient are higher than those for a smaller extinction coefficient with the same grid density. This is easily explained: since a sharper gradient of radiation intensity exists in the medium with a larger extinction coefficient, greater calculation errors will result than for simulations on the same grid density with smaller extinction coefficients.

### E. Gaussian shaped emissive field in a square enclosure

In this section, we pay special attention to the numerical stability of the LBM for radiative transfer. The radiative transfer in a square enclosure with an absorbing-emitting medium is considered. The emissive field of the medium has a Gaussian profile. This problem is described by the RTE [61] as

$$\mu\frac{dI}{dx} + \eta\frac{dI}{dy} + \kappa_a I = e^{-[\bar{s}(x,y)-c]^2/\alpha^2}, \quad x,y \in [0,1], \tag{53}$$

where the incident direction is selected to be $\mu = \eta = \sqrt{2}/2, \bar{s}(x,y) = (x+y)/\sqrt{2}$ is a distance parameter in the incident direction, and the emission profile parameters are

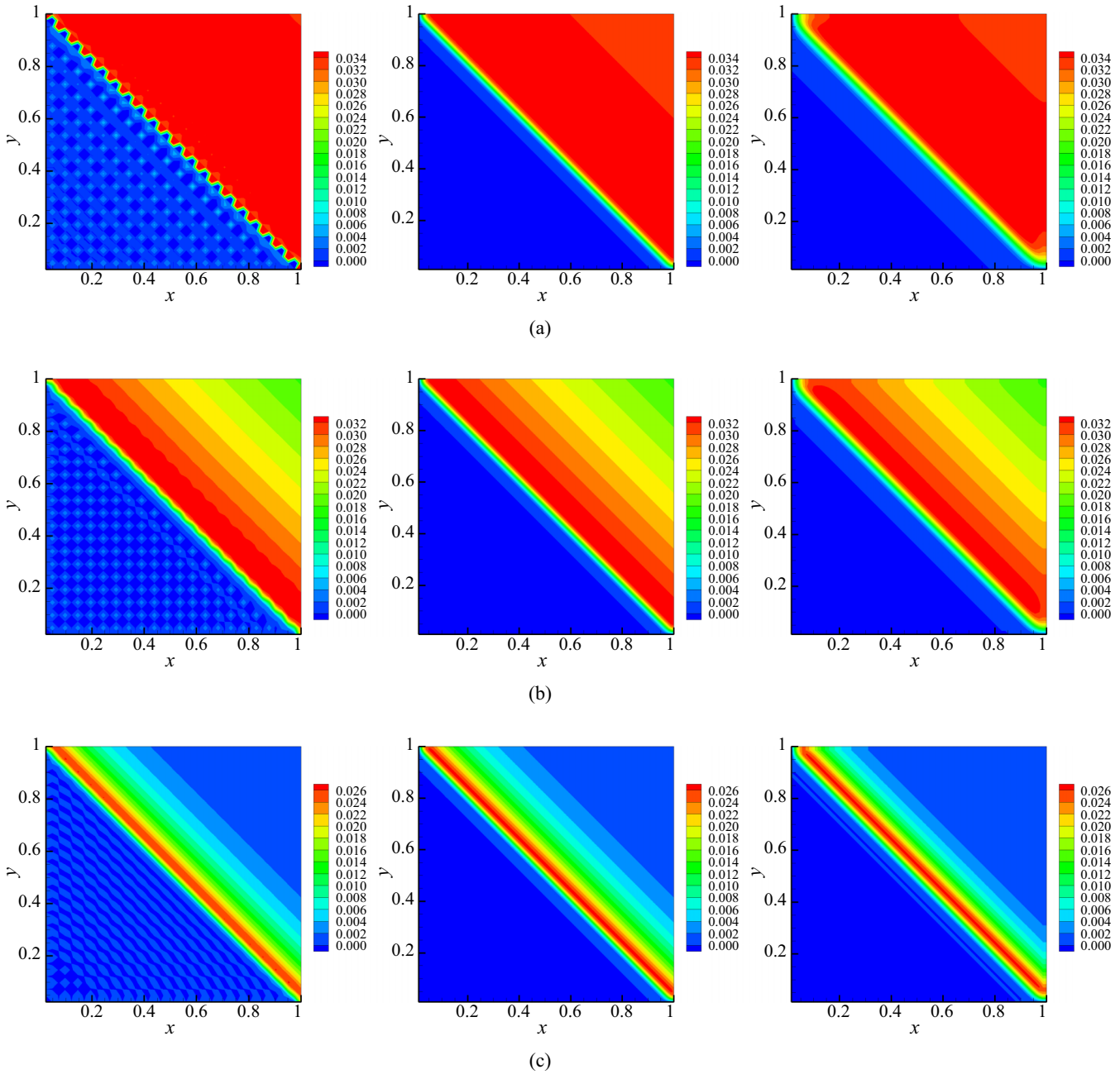


FIG. 8. Radiative intensity distributions obtained by the Galerkin FEM, an analytical solution, and the LBM (from left to right) for various absorbing coefficients. (a) $\kappa_a = 0.1\,\mathrm{m}^{-1}$, (b) $\kappa_a = 1\,\mathrm{m}^{-1}$, and (c) $\kappa_a = 10\,\mathrm{m}^{-1}$.

set as $c = \sqrt{2}/2$ and $\alpha = 0.02$. The boundary condition is prescribed on the inflow boundaries with null emission. An analytical solution can be obtained along the characteristic lines, written as

$$I(x,y) = \frac{\alpha\sqrt{\pi}}{2}\exp\{-\kappa_a[s(x,y) - c_s(x,y) - \alpha^2\kappa_a/4]\} \times \left\{\mathrm{erf}\left[\frac{\alpha\kappa_a}{2} + \frac{c_s(x,y)}{\alpha}\right] - \mathrm{erf}\left[\frac{\alpha\kappa_a}{2} + \frac{c_s(x,y) - s(x,y)}{\alpha}\right]\right\}, \quad (54)$$

where $s(x,y) = \frac{|x+y|-|x-y|}{\sqrt{2}}$ and $c_s(x,y) = \frac{1-|x-y|}{\sqrt{2}}$.

The radiative transfer problem is characterized by a large intensity distribution gradient in the enclosure. We solve the problem by using an analytic method and numerical techniques, and plot the radiation intensity distributions in the enclosure that result from Galerkin FEM, the analytical solution, and the LBM for different absorption coefficients ($\kappa_a = 0.1, 1, 10\mathrm{m}^{-1}$) in Fig. 8. The spatial resolutions used in the FEM and LBM are taken to be $41 \times 41$. As shown in Fig. 8, for small absorption coefficients, the spurious oscillations dominate the results and the intensity distribution obtained using the Galerkin FEM is almost totally spoiled in the left-lower triangular region of the enclosure where the intensity should be zero. The nonphysical oscillations are induced by an

intensity distribution with a large gradient, and with a higher absorption coefficient, they tend to become weaker. The results obtained by the LBM have no such spurious oscillations and maintain numerical stability. Due to the inherently transient nature of LBM simulations with a very small time interval, they primarily solve the distribution function of the particles by evolution (including collision and streaming steps) to obtain solutions for physical problems. Thus the LBM is more robust than the direct iterative solution of partial differential equations. To obtain stable solutions, the FEM requires special stabilization techniques, such as upwinding schemes to discretize the original RTE, or transforming the original RTE into a second-order equation [62].

### F. Coupled conduction and radiation problem

In this section we present an application of the proposed LBM to coupled radiative and conductive heat transfer to demonstrate that the LBM is highly adaptable to a multiphysics coupling problem. The problem of radiation coupled with conduction is of great interest in many fields of science and engineering, including the radiative cooling of a space droplet radiator, infrared heating and drying, the growth of optical crystals, the high-temperature use of ceramic components, highly backscattering protective insulation systems for reentry into atmosphere, and porous burners and insulation systems, as well as selected high-temperature components in advanced aircraft engines.

The energy equation for the problem can be expressed as follows:

$$\frac{\partial(\rho C_p T)}{\partial t} = \nabla \cdot (k \nabla T) - \nabla \cdot \mathbf{q}_R, \tag{55}$$

where $\rho$, $C_p$, $T$, $k$, and $\boldsymbol{q_R}$ are the density, specific heat, temperature, thermal conductivity, and radiative heat flux density, respectively.

The LB evolution equation for the temperature field can be expressed as

$$g_i(\mathbf{r} + \mathbf{e}_i \Delta t, t + \Delta t) - g_i(\mathbf{r},t) = -\frac{1}{\tau_T}\left[g_i(\mathbf{r},t) - g_i^{\mathrm{eq}}(\mathbf{r},t)\right] - \frac{\Delta t w_i}{\rho C_p} \nabla \cdot \mathbf{q}_R, \tag{56}$$

where $g_i$ is the temperature distribution function in the $i$ direction, $g_i^{\mathrm{eq}}$ is the equilibrium distribution function, and $\nabla \cdot \mathbf{q}_R = \beta(1-\omega)(4\sigma T^4 - G)$ is the radiative source term. The variable $\tau_T$ is the relaxation time for the temperature field,

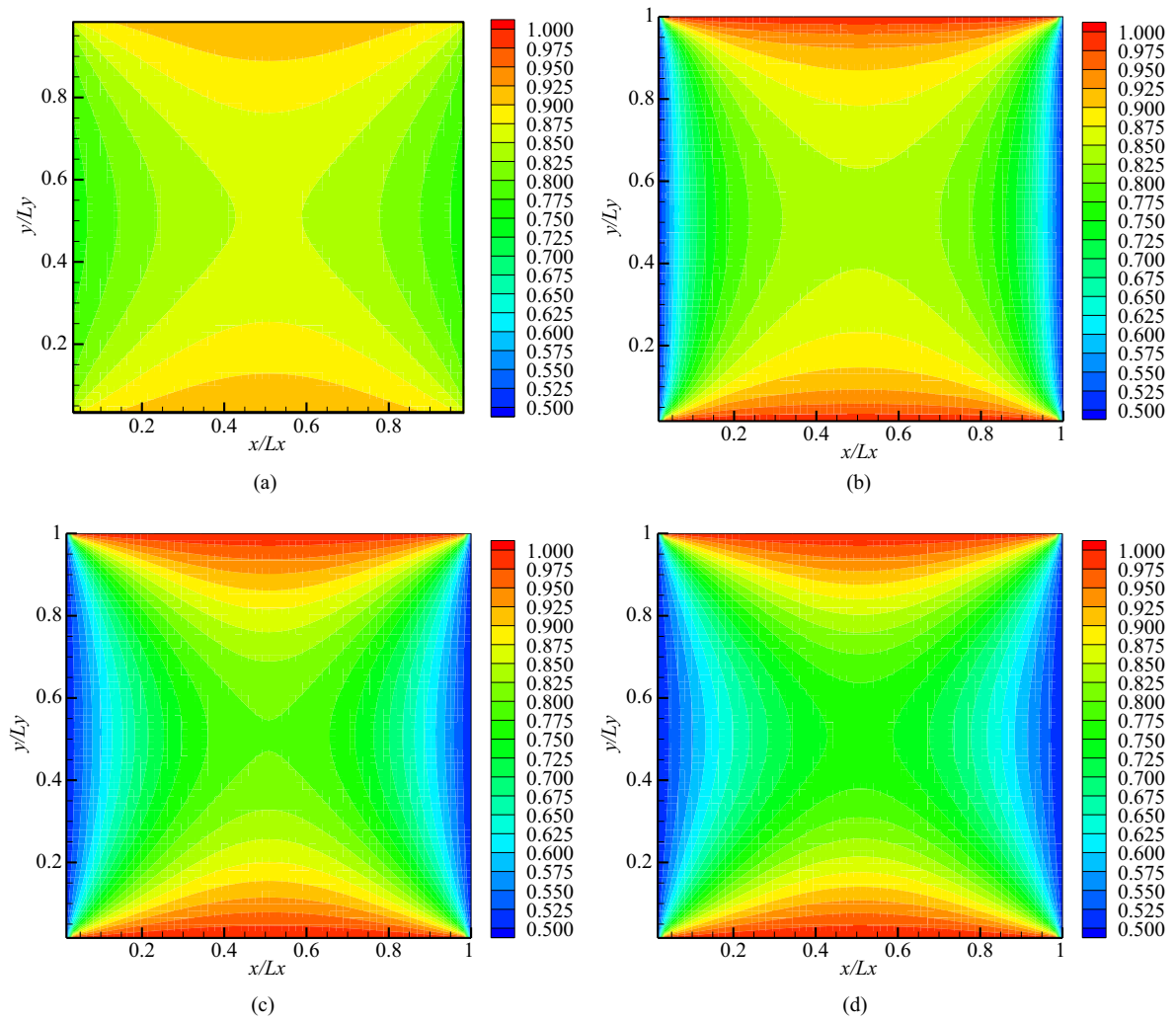


FIG. 9. Temperature distributions for various conduction-radiation parameters. (a) $Pl = 0$, (b) $Pl = 0.01$, (c) $Pl = 0.1$, and (d) $Pl = 1$.

represented by

$$\tau_T = \frac{\chi}{c_s^2 \Delta t} + \frac{1}{2}, \tag{57}$$

where $\chi = k/(\rho C_p)$ is the thermal diffusivity. The equilibrium distribution function is expressed by

$$g_i^{\mathrm{eq}} = T w_i, \tag{58}$$

and the macroscopic temperature can be computed from

$$T = \sum_i g_i. \tag{59}$$

The LBM is used to simulate coupled conduction and radiation in a black square enclosure with a purely absorbing medium. The boundary temperatures are kept constant, and the absorption coefficient is $\kappa_a = 1\,\mathrm{m}^{-1}$. Initially, the entire system is at a constant temperature, and for $t > 0$ the temperatures of the south and north boundaries are raised to twice the initial temperature value. We apply the D2Q9 lattice model and uniform meshes of $60 \times 60$ in the LB models for both conduction and radiation. The solution procedure can be briefly described as follows. Firstly, we calculate the radiative intensity field using Eq. (17) combined with Eq. (25) and obtain the incident radiation from Eq. (7). Secondly, we calculate the temperature field using Eq. (56) combined with Eq. (59) and obtain a new blackbody radiative intensity distribution. Finally, the steps are repeated until the convergence criterion is satisfied. In the solution procedure, the boundary conditions for both the temperature field and the radiative intensity field are evaluated using Eq. (48).

The steady-state temperature distributions are plotted in Fig. 9 for various conduction-radiation parameters $Pl$ [$Pl = k\kappa_{\mathrm{a}}/(4\sigma T_{\mathrm{ref}}^3)$, where $T_{\mathrm{ref}}$ is the average of the highest wall temperature and the lowest wall temperature]. Figure 9(a) shows temperature glides at the walls of the enclosure with $Pl = 0$. In the case where $Pl = 0$, no conduction contributes to the heat transfer, and the medium is at radiative equilibrium. The temperature glide is a characteristic phenomenon of heat transfer at radiative equilibrium and disappears in coupled radiation and conduction. With the increase of $Pl$, as shown in Figs. 9(b)–9(d), the contribution of thermal radiation decreases, and the temperature level consequently falls. The temperature distribution also tends to be nonuniform.

The simulations are carried out within a unified computational framework based on the LBM. In the unified computational framework, the lattice Boltzmann evolution equations for temperature fields and radiative intensity fields are similar, and for finding the fields, the same boundary condition implementation, lattice spacing, and discrete velocity model (D2Q9 scheme) are applied.

## V. CONCLUSIONS

A lattice Boltzmann model is proposed for a two-dimensional steady radiative transfer equation. To build a complete LB model, an artificial diffusion term is introduced to the radiative transfer equation. Based on the Chapman-Enskog expansion, the correct equilibrium distribution function and relaxation time expression are constructed for the corresponding lattice Boltzmann equation. From the expression of relaxation time, we see that the derived lattice Boltzmann equation with a relaxation time of 0.5 is exactly suitable for a standard steady radiative transfer equation.

Three test cases of radiative transfer are used as examples to validate the LBM. These test cases include a purely absorbing medium in a black enclosure with different extinction coefficients, a purely scattering medium in a gray enclosure with different wall emissivity, and an anisotropically scattering medium in a black enclosure with different scattering albedos. The radiative flux and incident radiation obtained by the LBM are comparable to those obtained by other numerical methods. The comparisons show that the lattice Boltzmann method proposed in this article achieves a high accuracy in solving two-dimensional radiative transfer problems. The spatial convergence property of the present LBM is thoroughly explored, and we find that the convergence rate of the LBM is dependent on the transport properties of the radiative transfer equation. With a large optical thickness, the radiative transfer equation can be regarded as a diffusion-dominated equation, and the LBM has a second-order convergence rate in space. With a decrease of optical thickness, convection characteristics of the radiative transfer equation become more significant, and the order of convergence rate for the LBM decreases accordingly. For an optical thickness of $\beta L = 1$, the order is approximately 1.7; for $\beta L = 10$, the order is 1.92; and if the optical thickness is further increased from 10, the order is increased to 2. The radiative transfer inside a square enclosure with a Gaussian shaped emissive field is also investigated, and the results obtained by the FEM and LBM are compared in detail. From the comparison, we see that the LBM has excellent numerical stability while the FEM solutions suffer from nonphysical oscillations. Finally, we present an application of the proposed LBM to coupled radiative and conductive heat transfer.

From the multiscale analysis based on the Chapman-Enskog expansion, we can see that the extension of the LB model to a three-dimensional radiative transfer equation is straightforward. In future works, we will extend the proposed LB model to radiative transfer in an irregular enclosure with participating media and multidimensional vector radiative transfer. We will also attempt to establish a unified framework based on the LBM to solve the coupling problem of multiphysics fields with the consideration of radiation.

## ACKNOWLEDGMENTS

This work has been supported by the National Natural Science Foundation of China (Grants No. 51421063 and No. 51422602) and the Fundamental Research Funds for the Central Universities (Grant No. HIT. IBRSEM. A. 201413).

[1] J. R. Howell, J. Heat Transfer **120**, 547 (1998).
[2] M. F. Modest, J. Heat Transfer **125**, 57 (2003).
[3] R. Kong, M. Ambrose, and J. Spanier, J. Comput. Phys. **227**, 9463 (2008).

[4] H. C. Hottel and E. S. Cohen, AIChE J. **4**, 3 (1958).
[5] J. M. Goyheneche and J. F. Sacadura, J. Heat Transfer **124**, 696 (2002).
[6] J. Yang and M. F. Modest, J. Quant. Spectrosc. Radiat. Transfer **104**, 217 (2007).
[7] R. Vaillon, M. Lallemand, and D. Lemonnier, J. Quant. Spectrosc. Radiat. Transfer **55**, 7 (1996).
[8] P. J. Coelho, J. Quant. Spectrosc. Radiat. Transfer **73**, 231 (2002).
[9] C. T. Salinas, Int. J. Therm. Sci. **49**, 302 (2010).
[10] H. Amiri, S. H. Mansouri, and P. J. Coelho, Int. J. Numer. Methods Heat Fluid Flow **22**, 862 (2012).
[11] B. Hunter and Z. Guo, Numer. Heat Transfer, Part B **63**, 485 (2013).
[12] J. C. Chai, H. S. Lee, and S. V. Patankar, J. Thermophys. Heat Transfer **8**, 419 (1994).
[13] B. Hunter and Z. Guo, Heat Transfer Eng. **37**, 341 (2016).
[14] S. Brandon and J. J. Derby, Int. J. Numer. Methods Heat Fluid Flow **2**, 299 (1992).
[15] L. H. Liu, L. Zhang, and H. P. Tan, J. Quant. Spectrosc. Radiat. Transfer **97**, 436 (2006).
[16] L. H. Liu, Int. J. Heat Mass Transfer **49**, 219 (2006).
[17] C. A. Wang, H. Sadat, V. Ledez, and D. Lemonnier, Int. J. Therm. Sci. **49**, 2282 (2010).
[18] S. Succi, M. Vergassola, and R. Benzi, Phys. Rev. A **43**, 4521 (1991).
[19] S. Y. Chen, H. D. Chen, D. Martinez, and W. Matthaeus, Phys. Rev. Lett. **67**, 3776 (1991).
[20] M. J. Pattison, K. N. Premnath, N. B. Morley, and M. A. Abdou, Fusion Eng. Des. **83**, 557 (2008).
[21] T. Inamuro, N. Konishi, and F. Ogino, Comput. Phys. Commun. **129**, 32 (2000).
[22] M. C. Sukop and D. Or, Phys. B **338**, 298 (2003).
[23] M. C. Sukop, H. Huang, C. L. Lin, M. D. Deo, K. Oh, and J. D. Miller, Phys. Rev. E **77**, 026710 (2008).
[24] Z. Yu and L. S. Fan, Phys. Rev. E **82**, 046708 (2010).
[25] B. Li and D. Y. Kwok, J. Chem. Phys. **120**, 947 (2004).
[26] M. R. Wang and Q. J. Kang, J. Comput. Phys. **229**, 728 (2010).
[27] Z. H. Chai, Z. L. Guo, and B. C. Shi, J. Appl. Phys. **101**, 104913 (2007).
[28] M. R. Wang, J. K. Wang, and S. Y. Chen, J. Comput. Phys. **226**, 836 (2007).
[29] X. G. Yang, B. C. Shi, Z. H. Chai, and Z. L. Guo, J. Sci. Comput. **61**, 222 (2014).
[30] K. Luo, J. Wu, H. L. Yi, and H. P. Tan, Phys. Rev. E **93**, 023309 (2016).
[31] M. Sheikholeslami, M. Gorji-Bandpy, and G. Domairry, Appl. Math. Mech. **34**, 833 (2013).
[32] A. Karimipour, M. H. Esfe, M. R. Safaei, D. T. Semiromi, S. Jafari, and S. N. Kazi, Phys. A **402**, 150 (2014).
[33] A. Karimipour, A. H. Nezhad, A. D'Orazio, M. H. Esfe, M. R. Safaei, and E. Shirani, Eur. J. Mech., B: Fluids **49**, 89 (2015).
[34] M. Sheikholeslami, H. R. Ashorynejad, and P. Rana, J. Mol. Liq. **214**, 86 (2016).
[35] D. Chatterjee and S. Chakraborty, Phys. Lett. A **341**, 320 (2005).
[36] A. Maroufi and C. Aghanajafi, J. Quant. Spectrosc. Radiat. Transfer **116**, 145 (2013).
[37] J. M. Fuentes, F. Kuznik, K. Johannes, and J. Virgone, Phys. Lett. A **378**, 374 (2014).
[38] Y. T. Huo and Z. H. Rao, Int. J. Heat Mass Transfer **86**, 197 (2015).
[39] P. Asinari, S. C. Mishra, and R. Borchiellini, Numer. Heat Transfer, Part B **57**, 126 (2010).
[40] S. C. Mishra, H. Poonia, R. R. Vernekar, and A. K. Das, Heat Transfer Eng. **35**, 1267 (2014).
[41] Y. Ma, S. K. Dong, and H. P. Tan, Phys. Rev. E **84**, 016704 (2011).
[42] H. Bindra and D. V. Patil, Phys. Rev. E **86**, 016706 (2012).
[43] Y. Zhang, H. L. Yi, and H. P. Tan, Opt. Express **21**, 24532 (2013).
[44] A. Mink, G. Thäter, H. Nirschl, and M. J. Krause, J. Comput. Sci. (in press).
[45] B. C. Shi and Z. L. Guo, Phys. Rev. E **79**, 016701 (2009).
[46] C. Huber, B. Chopard, and M. Manga, J. Comput. Phys. **229**, 7956 (2010).
[47] H. L. Lai and C. F. Ma, Phys. Rev. E **84**, 046708 (2011).
[48] F. F. Wu, W. P. Shi, and F. Liu, Commun. Nonlinear Sci. Numer. Simul. **17**, 2776 (2012).
[49] Z. H. Chai and T. S. Zhao, Phys. Rev. E **87**, 063309 (2013).
[50] Q. H. Li, Z. H. Chai, and B. C. Shi, J. Sci. Comput. **61**, 308 (2014).
[51] Q. H. Li, Z. H. Chai, and B. C. Shi, Comput. Math. Appl. **70**, 548 (2015).
[52] R. Z. Huang and H. Y. Wu, Phys. Rev. E **91**, 033302 (2015).
[53] J. D. Sterling and S. Y. Chen, J. Comput. Phys. **123**, 196 (1996).
[54] Z. L. Guo, C. G. Zheng, and B. C. Shi, Chin. Phys. **11**, 366 (2002).
[55] R. Koch and R. Becker, J. Quant. Spectrosc. Radiat. Transfer **84**, 423 (2004).
[56] W. A. Fiveland and J. P. Jessee, J. Thermophys. Heat Transfer **8**, 426 (1994).
[57] A. C. Ratzel and J. R. Howell, J. Heat Transfer **105**, 333 (1983).
[58] W. A. Fiveland, J. Heat Transfer **106**, 699 (1984).
[59] T. K. Kim and H. Lee, Int. J. Heat Mass Transfer **31**, 1711 (1988).
[60] J. H. Ferziger and M. Peric, *Computational Methods for Fluid Dynamics* (Springer Science & Business Media, Berlin, 2012).
[61] J. M. Zhao, J. Y. Tan, and L. H. Liu, J. Comput. Phys. **232**, 431 (2013).
[62] J. M. Zhao and L. H. Liu, Numer. Heat Transfer, Part B **51**, 391 (2007).